



Cite this: *RSC Adv.*, 2022, 12, 8310

# Effect of core–shell nanocomposites on the mechanical properties and rheological behaviors of cement pastes

Gang Wang,<sup>a</sup>  <sup>ab</sup> Hua Tan,<sup>a</sup> Chunjing Lu<sup>c</sup> and Ao Sun<sup>d</sup>

SiO<sub>2</sub> nanoparticles (50 nm in diameter) coated with poly(ethylene glycol) methyl ether methacrylate (PEGMA) were synthesized by radical polymerization. The SiO<sub>2</sub>/PEGMA nanocomposites were characterised using FITR, <sup>1</sup>HNMR and TGA methods. The load of PEGMA in SiO<sub>2</sub>/PEGMA nanocomposites was 72.9 wt%. The hydration products, microstructure, pore structure, density, compressive strengths and rheological properties of cement were investigated. The SiO<sub>2</sub>/PEGMA nanocomposite could not only significantly improve the cement hydration and densify the microstructure by reducing the content of calcium hydroxide and promoting the production of calcium silicate hydrate, but also efficiently enhance the fluidity of the cement slurry. The compressive strength of cement with 2 wt% SiO<sub>2</sub>/PEGMA nanocomposites was increased by 40.1% curing for 28 days, which was much better than cement with the physical blending of SiO<sub>2</sub> nanoparticles and superplasticizers. The SiO<sub>2</sub>/PEGMA nanocomposites with core–shell structure novelly combine the advantages of SiO<sub>2</sub> nanoparticles and superplasticizers to significantly improve the performance of cement pastes. The results obtained provide a new understanding of the effect of the core–shell nanocomposites on cement pastes and demonstrate the potential of the nanocomposites for well cementing applications.

Received 23rd December 2021

Accepted 10th March 2022

DOI: 10.1039/d1ra09283a

rsc.li/rsc-advances

## 1. Introduction

During well cementing, oil well cement used to provide well integrity is susceptible to formation stress, periodic external pressure changes, and the difference in elasticity between the cement sheath and casing during the production of wells.<sup>1–4</sup> These stresses and pressures may produce unbalanced forces in the cement stone, causing brittle fracture or the formation of micro-annulus and micro-cracks.<sup>5</sup> The destruction of the downhole cement sheath seriously affects the productivity and production safety of wells.<sup>6,7</sup> With the deepening of oilfield exploration and development, the requirements for the performance of oil well cement are getting higher and higher to meet the needs of cementing technology under complex geological conditions.

Silica fume is a by-product of the ferroalloy industry, and its particle size is about 0.1–0.5 μm.<sup>8,9</sup> In addition, the main component of silica fume is amorphous silica, so the pozzolanic

activity is higher than that of other mineral admixtures.<sup>10</sup> The effect of silica fume in cement is similar to that of SiO<sub>2</sub> nanoparticles.<sup>11</sup> Compared with silica fume, SiO<sub>2</sub> nanoparticles have more significant advantages in pozzolanic effect, filling effect and nucleation ability in cement.<sup>12</sup> SiO<sub>2</sub> nanoparticles are higher pozzolanic activity than silica fume and can react with calcium hydroxide to generate extra calcium silicate hydrate (C–S–H).<sup>13</sup> In addition, the particle sizes of SiO<sub>2</sub> nanoparticles are smaller than that of silica fume, SiO<sub>2</sub> nanoparticles can fill smaller pores in nanoscale, thereby densifying the pore structure of cement.<sup>14</sup> Besides, SiO<sub>2</sub> nanoparticles can act as nucleation sites for C–S–H to greatly accelerate the hydration in the early stage.<sup>15</sup> Additionally, the presence of SiO<sub>2</sub> nanoparticles in cement pastes can effectively improve their rheological properties.<sup>16,17</sup> However, SiO<sub>2</sub> nanoparticles have a strong tendency to agglomerate, which can easily form weak zones in oil well cement, reducing the mechanical properties of cement.<sup>18–20</sup> As a result, the application of SiO<sub>2</sub> nanoparticles in cementing is restricted. The dispersion of SiO<sub>2</sub> nanoparticles can be improved by surface modification of nano-SiO<sub>2</sub>.

The dispersion stability of SiO<sub>2</sub> nanoparticles in oil well cement can be improved by adding superplasticizers, which was different types of polymers, such as phosphate polycarboxylate superplasticizers, polycarboxylate superplasticizers and polyether-based superplasticizers.<sup>21,22</sup> The superplasticizers can adsorb cement particles through the branched chains, which significantly improves the rheological behaviors, accelerates the

<sup>a</sup>Guangdong Provincial Key Laboratory of Petrochemical Pollution Process and Control, Guangdong University of Petrochemical Technology, Maoming 525000, China. E-mail: wghill@126.com

<sup>b</sup>School of Chemistry, Guangdong University of Petrochemical Technology, Maoming 525000, China

<sup>c</sup>School of Petroleum Engineering, Northeast Petroleum University, Daqing 163318, China

<sup>d</sup>Center of Chemistry for Frontier Technologies, Zhejiang University, Hangzhou 310058, China


hydration process, and reinforces the mechanical properties of cement.<sup>23–25</sup> Rheological behaviors of the oil well cement are the main factors that decide the borehole sealing effectiveness.<sup>26</sup> However, the interaction between SiO<sub>2</sub> nanoparticles and superplasticizers is weak, which cannot essentially change the strong agglomeration trend of SiO<sub>2</sub> nanoparticles, thus the uniform dispersion of SiO<sub>2</sub> nanoparticles in oil well cement cannot be achieved on the nanoscale level.<sup>27</sup>

With the maturity of nanotechnology in recent years, nanocomposite materials have been widely used in different research fields, and polymer/nanoparticles composite materials have become the focus of scientific research in this century.<sup>28–30</sup> The mechanical and thermodynamic properties of the composites were greatly improved by introducing nanoparticles into the polymer matrix.<sup>31–33</sup> Numerous studies have shown that, compared with the physical blending of polymer and nanoparticles, polymer/nanoparticle composites have been greatly improved in mechanical properties, thermal properties, electrical properties, rheological properties, flame-retardant, anti-corrosive properties.<sup>34–37</sup> SiO<sub>2</sub> nanoparticles with grafted polymers possessed excellent dispersion stability due to steric hindrance and electrostatic repulsion,<sup>38–41</sup> which probably resulted in better properties of oil well cement. And the grafted polymers can endow the nanocomposite with multiple properties.

In the present study, SiO<sub>2</sub> nanoparticles coated with PEGMA (SiO<sub>2</sub>/PEGMA) were prepared by radical polymerization, and the effect of the SiO<sub>2</sub>/PEGMA nanocomposites on the hydration process, mechanical and rheological properties of cement was investigated. Hydration products composition, microstructure, density and pore structure of cement were characterised to investigate the reinforcement mechanism by means of TGA, SEM and MIP, respectively. Compressive strengths and rheological properties were also studied as important indicators for cement.

## 2. Experimental

### 2.1 Materials

SiO<sub>2</sub> nanoparticles (50 nm) and anhydrous ethanol were purchased from the Sinopharm Chemical Reagent Company. *N,O*-bis-(trimethylsilyl) acetamide (BSA), poly(ethylene glycol) methyl ether methacrylate (PEGMA), 2,2'-azobisisobutyronitrile (AIBN) were purchased from Sigma Aldrich. Polycarboxylic acid superplasticizer (PEGMA/AA) was received from cementing technology service center of Sinopec Shengli Petroleum Engineering Co., Ltd, Dongying, China. Cementitious materials were class G oil well cement from Zhongchang Special Cement Co., Ltd, Zibo, China, of which the compositions were presented in Table 1. All products were used as received.

Table 1 Chemical compositions of the oil well cement (%)

SiO <sub>2</sub>	Al <sub>2</sub> O <sub>3</sub>	Fe <sub>2</sub> O <sub>3</sub>	CaO	MgO	K <sub>2</sub> O	SO <sub>3</sub>	MnO <sub>2</sub>	Loss on ignition
23.2	3.5	4.5	66.1	1.0	0.3	1.1	0.1	0.2

### 2.2 Preparation of SiO<sub>2</sub>/PEGMA

2 wt% SiO<sub>2</sub> nanoparticles in 10 wt% ethanol solution were sonicated for 15 min to achieve the homogeneous suspension. 3 wt% BSA was added to the above dispersion and stirred for 6 h at 50 °C under nitrogen. After cooling to atmospheric temperature, the dispersion was centrifuged and washed by alcohol multiple times to remove the unreacted BSA. Subsequently, the modified SiO<sub>2</sub> nanoparticles (SiO<sub>2</sub>-BSA) were dried at 60 °C for 15 h.

2 wt% SiO<sub>2</sub>-BSA in anhydrous ethanol was sonicated for 30 min to uniform dispersion. 10 wt% PEGMA and 0.025 wt% AIBN were added to the dispersion and mixed for 4 h under nitrogen at 60 °C. Thereafter, the obtained product was centrifuged and rinsed several times with alcohol and labelled as SiO<sub>2</sub>/PEGMA nanocomposites. The preparation process for this nanocomposite is illustrated in Fig. 1. The chemical structure of synthesized SiO<sub>2</sub>/PEGMA nanocomposites was then characterised by FTIR spectrometry and <sup>1</sup>HNMR spectroscopy techniques.

### 2.3 Preparation of cement samples

Four kinds of cement samples were prepared to study the influence of SiO<sub>2</sub>/PEGMA nanocomposites on the performance of oil well cement, including blank oil well cement, oil well cement with 2 wt% SiO<sub>2</sub> nanoparticles, oil well cement with 2 wt% SiO<sub>2</sub> nanoparticles and 0.3 wt% PEGMA/AA superplasticizer, oil well cement with 2 wt% SiO<sub>2</sub>/PEGMA nanocomposites. These samples were labelled as blank, SiO<sub>2</sub>, SiO<sub>2</sub> + P and SiO<sub>2</sub>/PEGMA, respectively.

### 2.4 Compressive strength measurement

The compressive strength of set cement was evaluated according to the GB/T 19139-2012 National Standard of China. The prepared cement pastes having a water–cement ratio of 0.44 was poured into a cubic copper mold with a side length of 50.8 mm and cured at 75 °C and 21 MPa for a period of time. The curing time was set to 3, 7 and 28 days, respectively. The compressive strength of hardened cement pastes was tested under a loading rate of 72 kN min<sup>−1</sup> by the triaxial rock mechanics testing system (TAW-1000, China). The compressive strength of cement samples at each curing time was tested 5 times.

### 2.5 Density of cement samples

The dry mass of cement samples with a curing time of 3 days was measured after vacuum drying at 105 °C for 12 h. The bulk density of cement could be written as follows:

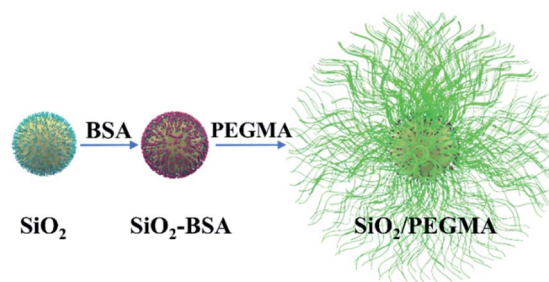


Fig. 1 The synthesis route of SiO<sub>2</sub> nanoparticles coated with PEGMA.



$$\rho = \frac{M}{V} \quad (1)$$

where  $M$  and  $V$  are the dry mass (g) and specimen volume ( $\text{cm}^3$ ) of the cement samples, respectively. All results were the arithmetical average of 3 parallel tests.

## 2.6 Rheological behavior of cement paste

Rotary rheometer (MCR 302 with parallel plates, Austria) was utilised to analyse the rheological properties of cement paste based on API Recommended Practice 10B-2, where the plates gap and plate diameter were selected as 2 mm and 25 mm, respectively. The cement pastes having a water–cement ratio of 0.44 was stirred for 2 min before performing the rheological test. The test was kept 25 °C through a water circulation system around the sample container.

## 2.7 Characterization

Thermogravimetric analysis (TGA, TA 5200, USA) was applied to determine the weight loss of the  $\text{SiO}_2$ /PEGMA nanocomposites and cement with a curing time of 3 days. Scanning electron microscope (SEM, IT100, Japan) was utilised to observe the microstructure of oil well cement after curing for 3 days. Mercury intrusion porosimeter (MIP, AutoPore III, USA) was applied to characterise the pore structure of hardened cement pastes with a curing time of 3 days.

# 3. Results and discussion

## 3.1 Characterisation of $\text{SiO}_2$ /PEGMA nanocomposites

The FTIR spectra of the  $\text{SiO}_2$  nanoparticles,  $\text{SiO}_2$ -BSA, and  $\text{SiO}_2$ /PEGMA nanocomposites were shown in Fig. 2(a). For the  $\text{SiO}_2$  nanoparticles, 1100 and 1675  $\text{cm}^{-1}$  were corresponded to the Si–O–Si and bending vibration of  $\text{H}_2\text{O}$ , respectively. The peak centred at 3450  $\text{cm}^{-1}$  was ascribed to the presence of Si–OH. The spectra of  $\text{SiO}_2$ -BSA exhibited a new absorption band at 2950  $\text{cm}^{-1}$ , which was attributed to the stretching vibration of the C–H bond due to the presence of BSA. Compared with the  $\text{SiO}_2$ -BSA, the absorption band around 1575  $\text{cm}^{-1}$  in  $\text{SiO}_2$ /PEGMA nanocomposites can correspond to C=O, and the intensity of absorption peaks at 3450  $\text{cm}^{-1}$  is significantly enhanced, which confirms that PEGMA has been grafted to  $\text{SiO}_2$  nanoparticles.

To further verify the successful preparation of the  $\text{SiO}_2$ /PEGMA nanocomposites,  $^1\text{H}$ NMR was carried out and illustrated in Fig. 2(b). The peaks centred at 1.08 and 1.75 ppm were related to the  $-\text{CH}_3$  and  $-\text{CH}_2$ , respectively. Besides, the peak values at 3.26 and 3.59 ppm were ascribed to the  $\text{O}-\text{CH}_3$  and  $-\text{CH}_2-\text{CH}_2-\text{O}$ . The above characteristic peaks of PEGMA were found in the  $^1\text{H}$ NMR spectrum of  $\text{SiO}_2$ /PEGMA nanocomposites, further confirming the successful preparation of final nanocomposites.

The TGA curves of  $\text{SiO}_2$ ,  $\text{SiO}_2$ -BSA and  $\text{SiO}_2$ /PEGMA were illustrated in Fig. 3. For the  $\text{SiO}_2$ -BSA, the mass loss embraced two parts, specifically one slightly dwindled in the temperature range between 30 and 200 °C while the other diminished in the region 200–510 °C due to the decomposition of chemically

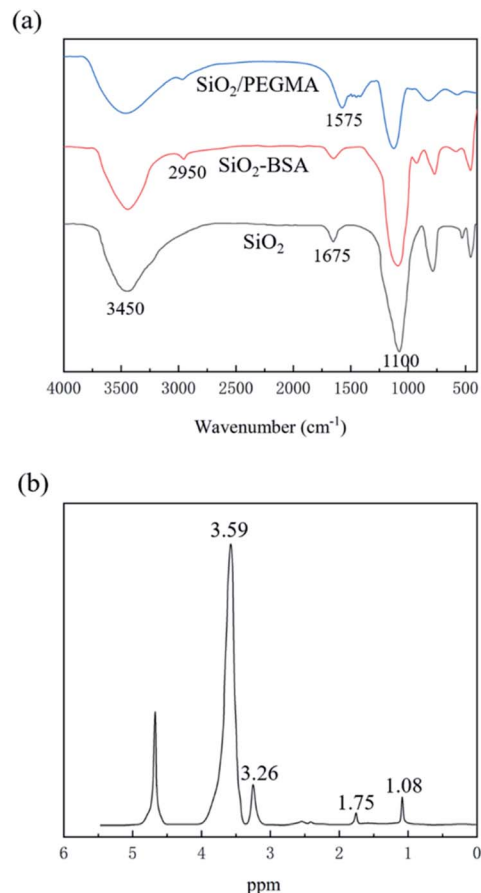


Fig. 2 IR spectra of  $\text{SiO}_2$ ,  $\text{SiO}_2$ -BSA and  $\text{SiO}_2$ /PEGMA (a);  $^1\text{H}$ NMR spectra of  $\text{SiO}_2$ /PEGMA (b).

bonded BSA from the particle surface. The  $\text{SiO}_2$ /PEGMA has a significant weight loss within the temperature range of 220–420 °C, mainly due to the decomposition of PEGMA. The weight percentage of PEGMA on the  $\text{SiO}_2$  nanoparticles can be written as eqn (2):

$$\Delta W_{\text{PEGMA}} = W_{220, \text{SiO}_2/\text{PEGMA}} - W_{420, \text{SiO}_2/\text{PEGMA}} - (W_{220, \text{SiO}_2-\text{BSA}} - W_{420, \text{SiO}_2-\text{BSA}}) \quad (2)$$

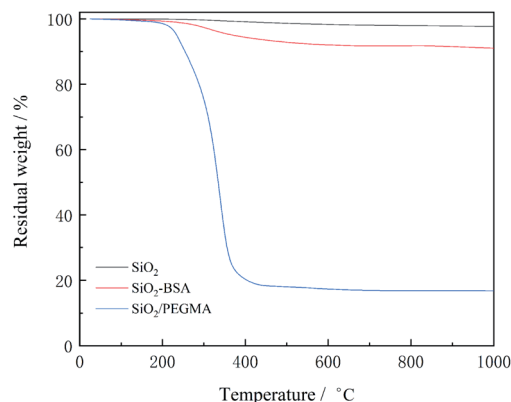


Fig. 3 TGA curves of  $\text{SiO}_2$ ,  $\text{SiO}_2$ -BSA and  $\text{SiO}_2$ /PEGMA.



where  $\Delta W_{\text{PEGMA}}$  is the amount of PEGMA on the  $\text{SiO}_2$  nanoparticles.  $W_{220, \text{SiO}_2\text{-BSA}}$  and  $W_{420, \text{SiO}_2\text{-BSA}}$  are the respective  $\text{SiO}_2$ -BSA residual weight at 220 and 420 °C.  $W_{220, \text{SiO}_2/\text{PEGMA}}$  and  $W_{420, \text{SiO}_2/\text{PEGMA}}$  are the respective  $\text{SiO}_2/\text{PEGMA}$  residual weight at 220 and 420 °C. The load of PEGMA in  $\text{SiO}_2/\text{PEGMA}$  calculated from the above equation was 72.9 wt%. After anchoring BSA to the surface of  $\text{SiO}_2$  nanoparticles, PEGMA formed a shell structure on the nanoparticle surface.

### 3.2 Thermal gravimetric analysis

The TGA curves for blank,  $\text{SiO}_2$ ,  $\text{SiO}_2 + \text{P}$  and  $\text{SiO}_2/\text{PEGMA}$  cement samples after curing for 3 days was shown in Fig. 4. The  $\text{SiO}_2/\text{PEGMA}$  nanocomposite was more effective in promoting the hydration process of cement and reducing the content of CH in the hydration process. According to the TGA curves, the mass loss of the samples at 400–500 °C was caused by the decomposition of CH, and the mass loss of CH ( $M_{\text{CH}}$ ) can be written as follows:

$$M_{\text{CH}} = \frac{74}{18} \times W_{\text{CH}} \quad (3)$$

where  $W_{\text{CH}}$  is the mass loss of the samples at 400–500 °C.<sup>42</sup>

The hydration degree of oil well cement could be represented by the non-evaporable water content, which was the mass loss between 105 °C and 1000 °C, and  $M_{\text{non-evaporable}}$  is the content of non-evaporable water. According to Table 2, the mass of non-evaporable water of  $\text{SiO}_2/\text{PEGMA}$  is more than that in the rest of the cement, while the content of CH was lowest.  $\text{SiO}_2$  nanoparticles can decrease the crystal size and content of CH by reacting with CH, reducing the orientation of CH crystals aggregated at the interface and effectively improving the interface.<sup>43</sup> The pozzolanic reaction from  $\text{SiO}_2$  nanoparticles and CH

is beneficial to improve the mechanical properties of cement.<sup>20</sup>  $\text{SiO}_2$  nanoparticles aggregates due to their small size, affecting the pozzolanic activity.  $\text{SiO}_2$  nanoparticles grafted with PEGMA had a higher pozzolanic activity, which could significantly promote the hydration process of cement and consume CH to generate C-S-H.

### 3.3 Scanning electron micrograph analysis

The hardened cement pastes were also characterised by SEM, and the images were displayed in Fig. 5. It can be seen from Fig. 5(a) that the microstructure of blank cement was loose with a lot of holes and cracks, and the compactness was poor. As shown in Fig. 5(b), there were also many obvious pores in cement with  $\text{SiO}_2$  nanoparticles. According to Fig. 5(c), although the microstructure of  $\text{SiO}_2 + \text{P}$  cement stone became denser, a few holes can be still observed. According to Fig. 5(d), it had the densest microstructure without any obvious pores. The mechanical properties of cement depend on its microstructure.<sup>44</sup>  $\text{SiO}_2$  nanoparticles not only promote the hydration reaction and produces C-S-H to fill the pores of the cement paste, but also fill the voids between the grains in the cement matrix.<sup>20</sup>  $\text{SiO}_2$  nanoparticles were easy to agglomerate, resulting in a significant decrease in pozzolanic activity and nucleation effect.<sup>45</sup> The physical blending of  $\text{SiO}_2$  nanoparticles and PEGMA/AA, and grafting PEGMA on the surface of  $\text{SiO}_2$  nanoparticles improved the microstructure of cement. As for  $\text{SiO}_2 + \text{P}$ , the superplasticizers could improve the dispersion stability of  $\text{SiO}_2$  nanoparticles and accelerate the hydration process, which made the microstructure more compact. However, the interaction between  $\text{SiO}_2$  nanoparticles and superplasticizers is weak, resulting in the agglomeration of  $\text{SiO}_2$  nanoparticles in the cement slurry.<sup>27</sup> As for  $\text{SiO}_2/\text{PEGMA}$ , the  $\text{SiO}_2/\text{PEGMA}$  nanocomposites effectively optimized the microstructure of oil well cement. This may be mainly due to the core-shell structure of

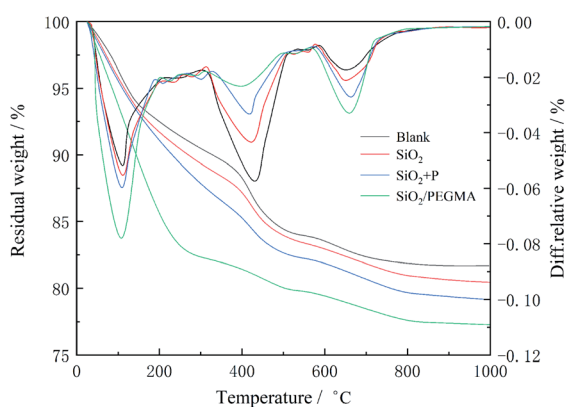


Fig. 4 TGA curves of four kinds of cement pastes.

**Table 2** The mass of non-evaporable water ( $M_{\text{non-evaporable}}$ ) and CH ( $M_{\text{CH}}$ ) of four kinds of cement pastes

Cement samples	$M_{\text{non-evaporable}}/\%$	$M_{\text{CH}}/\%$
Blank	$14.3 \pm 0.2$	$18.9 \pm 0.5$
$\text{SiO}_2$	$15.1 \pm 0.3$	$15.2 \pm 0.4$
$\text{SiO}_2 + \text{P}$	$15.4 \pm 0.2$	$11.9 \pm 0.3$
$\text{SiO}_2/\text{PEGMA}$	$16.5 \pm 0.1$	$6.8 \pm 0.4$

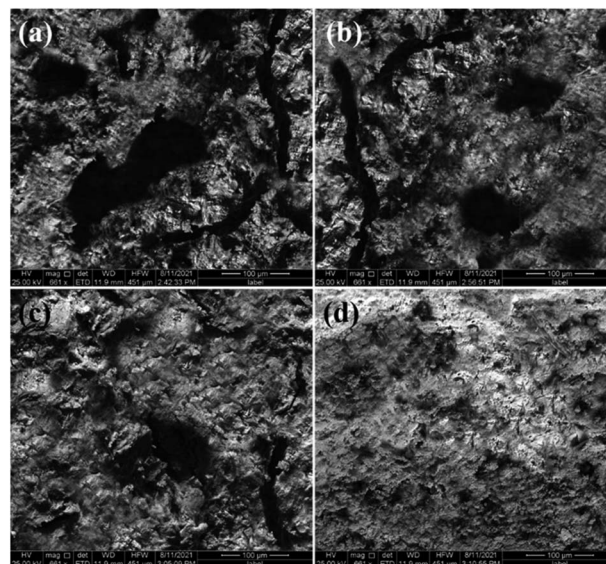


Fig. 5 SEM images: (a) blank cement; (b)  $\text{SiO}_2$  cement; (c)  $\text{SiO}_2 + \text{P}$  cement and (d)  $\text{SiO}_2/\text{PEGMA}$  cement.



SiO<sub>2</sub>/PEGMA nanocomposites which could significantly improve the pozzolanic activity and nucleation effect of SiO<sub>2</sub> nanoparticles.

### 3.4 Pore structure analysis

The hydration process of cement is transformed cement particles and water into a solid and low permeability material, which is a chemically driven process.<sup>46</sup> The microstructure of cement was heterogeneous and multiphase with different types of pores inside, including gel pores (3–10 nm), capillary pores (10–1000 nm) and large pores (>1000 nm).<sup>47</sup> As shown in Fig. 6 and Table 3, the pore size distribution, pore structure and density of cement samples were most affected by the addition of the SiO<sub>2</sub>/PEGMA nanocomposites. The density of cement with SiO<sub>2</sub>/PEGMA was the highest, reaching 2.32 g cm<sup>-3</sup>. According to the effect of pore size on cement properties, the pores are classified into harmless pores (<20 nm), less harmful pores (20–50 nm), harmful pores (50–200 nm) and more harmful pores (>200 nm).<sup>48</sup> The main peak of the pore size distribution of SiO<sub>2</sub>/PEGMA cement was obviously shifted to the left, and the value of the peak was the lowest. In addition, the total porosity and average pore diameter of SiO<sub>2</sub>/PEGMA decreased from 35.6% and 25.8 nm to 17.5% and 12.6 nm, respectively, which indicates that the SiO<sub>2</sub>/PEGMA nanocomposites had a dramatical refining effect on the pore structure of oil well cement. The main reason for improving the pore structure of cement was the filling effect and the pozzolanic reaction. SiO<sub>2</sub>/PEGMA nanocomposites with a small particle size and high pozzolanic activity could fill the pores in the nanoscale and produce C–S–H with CH to optimize the distribution of the pore structure. SiO<sub>2</sub>/

PEGMA nanocomposites could not only act as an activator to promote the hydration reaction, but also play a filling role to reduce the pore volume and make the cement more compact.

### 3.5 Mechanical properties analysis

The compressive strengths of these four cement samples after curing for 3, 5 and 28 days were presented in Fig. 7. The compressive strengths of all samples increased continuously with the prolonging of the curing time. Moreover, the compressive strengths of the cement with SiO<sub>2</sub> nanoparticles, the physical blending of SiO<sub>2</sub> nanoparticles and PEGMA/AA superplasticizer, and the SiO<sub>2</sub>/PEGMA nanocomposites after curing for 28 days increased by 9.1%, 15.4% and 40.1%, respectively. The main reason for improving the compressive strength of hardened cement pastes is the pozzolanic reaction, filling effect and nucleation ability of SiO<sub>2</sub>/PEGMA nanocomposites. The SiO<sub>2</sub> nanoparticles with grafting PEGMA could react with hydration products to generate additional C–S–H, fill up smaller holes to optimize the distribution of the pore structure, and act as nucleation sites for C–S–H in the early hydration stage to greatly accelerate the hydration of cement. These results further proved that the SiO<sub>2</sub> nanoparticles with core-shell structure could possess excellent pozzolanic activity, filling effect and nucleation ability to accelerate the hydration process and reinforce the mechanical properties of cement.

### 3.6 Rheological properties

Mixing well oil cement slurry exhibiting yield stress is one of the most challenging tasks during well cementing, and effectively reducing the yield pressure of cement can improve the cement operation.<sup>49</sup> To better clarify the effect of SiO<sub>2</sub>/PEGMA nanocomposite on the fluidity of oil well cement, the changes in shear stress of cement slurries as a function of shear rate were determined. It can be seen from Fig. 8, the shear stresses of the cement were approaching a similar value with the growth of the shear rate due to the solidification of the cement slurry. The modified Bingham model can better reflect the effect of very low shear stresses induced in the low shear rate region of flow

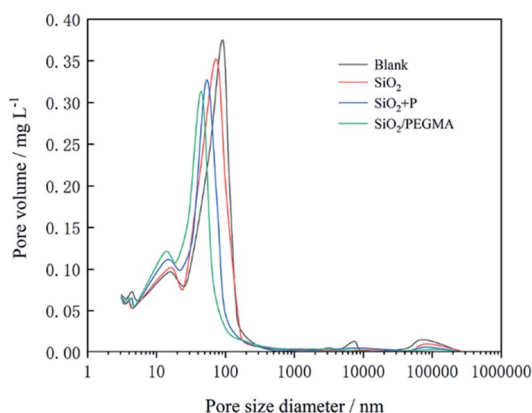


Fig. 6 Pore size distribution of four kinds of cement samples.

Table 3 Pore structure parameters and density of cement samples

Cement samples	Average pore diameter/nm	Total porosity/%	Density/g cm <sup>-3</sup>
Blank	25.8 ± 0.7	35.6 ± 1.2	2.14 ± 0.04
SiO <sub>2</sub>	21.7 ± 0.9	31.2 ± 0.9	2.21 ± 0.02
SiO <sub>2</sub> + P	18.1 ± 0.9	27.3 ± 1.1	2.25 ± 0.03
SiO <sub>2</sub> /PEGMA	12.6 ± 0.8	17.5 ± 0.8	2.32 ± 0.04

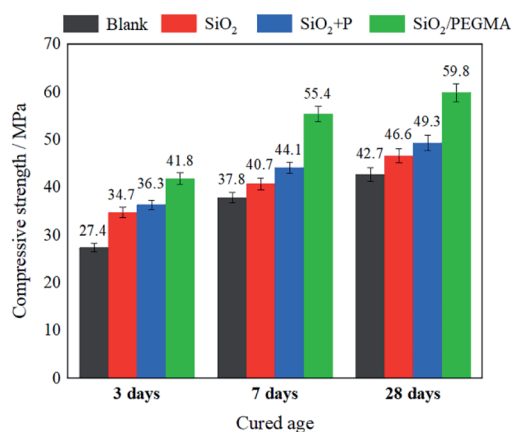


Fig. 7 Compressive strength of hardened cement pastes.



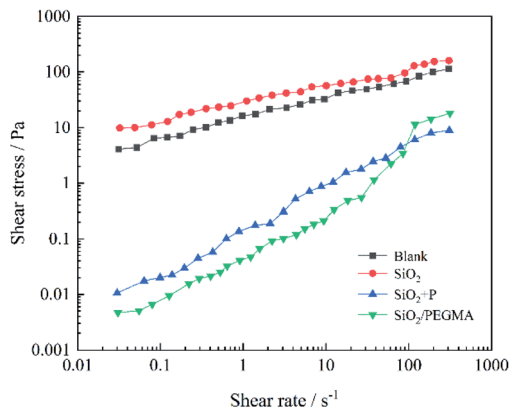


Fig. 8 Changes in shear stress with shear rate for four kinds of cement slurries.

curves.<sup>50</sup> The modified Bingham model can be written as follows:

$$\tau = \tau_0 + \mu_p \dot{\gamma} + c \dot{\gamma}^2 \quad (4)$$

where  $\tau$ ,  $\mu_p$ ,  $\dot{\gamma}$  and  $c$  are considered as the shear stress, plastic viscosity, shear rate and a regression constant, respectively. The modified Bingham model was used to estimate the rheological behavior of cement pastes. Shear stress of the blank cement suspension was about 3 Pa and steadied with the growth of the shear rate. The yield stress of cement suspension with  $\text{SiO}_2$  nanoparticles was highest among all samples, which was about 10 Pa. And with the increase of the shear rate, its shear stress decreased gradually to the value, which was slightly lesser than that of blank cement. As for the  $\text{SiO}_2 + \text{P}$  cement suspension, its yield stress is as low as 0.01 Pa. While for the cement suspension with  $\text{SiO}_2/\text{PEGMA}$  nanocomposites, its yield stress is even lower than that of the  $\text{SiO}_2 + \text{P}$  cement suspension. The  $\text{SiO}_2$  cement samples present higher yield stress than the blank cement due to the silica-silica interactions.<sup>51</sup> The adding PEGMA/AA improved the rheological behavior of the cement slurries due to the adsorption of active branched polymer sites onto the surface of cement grains. The grafted PEGMA of  $\text{SiO}_2/\text{PEGMA}$  nanocomposites could adsorb on the cement grains through its polyethylene glycol branch and play a substantial role in the fluidity of cement pastes to effectively reduce the yield stress of the cement suspension.

## 4. Conclusion

In this investigation, the  $\text{SiO}_2/\text{PEGMA}$  nanocomposites with core-shell structure were prepared by radical polymerization, and the load of PEGMA in  $\text{SiO}_2/\text{PEGMA}$  calculated from the above equation was 72.9 wt%. The hydration products, microstructures, mechanical and rheological properties of blank,  $\text{SiO}_2$ ,  $\text{SiO}_2 + \text{P}$  and  $\text{SiO}_2/\text{PEGMA}$  cement samples were studied by contrast analysis. The hydration degree of  $\text{SiO}_2/\text{PEGMA}$  was more than that in the rest of the cement, while the content of CH was lowest. The  $\text{SiO}_2/\text{PEGMA}$  nanocomposites were able to efficiently accelerate the hydration process by promoting the production of

C-S-H and decreasing  $\text{Ca}(\text{OH})_2$  content. The microstructure of  $\text{SiO}_2/\text{PEGMA}$  cement was the densest without any obvious pores, which was due to the higher pozzolan activity and filling effect of  $\text{SiO}_2/\text{PEGMA}$ . The density of cement with  $\text{SiO}_2/\text{PEGMA}$  was the highest, reaching  $2.32 \text{ g cm}^{-3}$ . In addition, the total porosity and average pore diameter of  $\text{SiO}_2/\text{PEGMA}$  decreased from 35.6% and 25.8 nm to 17.5% and 12.6 nm, respectively, which indicates that the  $\text{SiO}_2/\text{PEGMA}$  nanocomposites had a dramatical refining effect on the pore structure. The pozzolanic activity, nucleation effect and filling effect of  $\text{SiO}_2/\text{PEGMA}$  nanocomposites made the microstructure of the cement more compact and thus improved the mechanical properties of cement. The cement with  $\text{SiO}_2/\text{PEGMA}$  nanocomposites increased the compressive strength by 40.1% curing for 28 days, which was much better than other cement samples. The  $\text{SiO}_2$  nanoparticles with core-shell structure could promote the generation of more C-S-H by reacting with CH, fill the gaps between the cement grains to improve the microstructure of cement, and provide nucleation sites for hydration as well as the growth of hydrated products to greatly accelerate the hydration process. Besides, the modified Bingham model was used to estimate the rheological behavior of cement pastes. Compared with the physical blending of polymers and  $\text{SiO}_2$  nanoparticles,  $\text{SiO}_2/\text{PEGMA}$  nanocomposite can better improve the fluidity properties of cement slurries, and its yield stress is even lower than 0.01 Pa, which provided very suitable workability conditions. The  $\text{SiO}_2/\text{PEGMA}$  nanocomposites could not only significantly improve the cement hydration and densify the microstructure but also efficiently enhance the fluidity of the cement slurries. The core-shell structure endowed the nanocomposite with multiple functions show broad potential applications in the field of oil well cementing.

## Author contributions

All authors made critical contributions to the collection and interpretation of data. Gang Wang conceived and designed the experiments; Hua Tan and Chunjing Lu performed the experiments; Gang Wang and Ao Sun analysed the data; Gang Wang wrote the paper.

## Conflicts of interest

There is no conflict of interest to be reported.

## Acknowledgements

This study was funded by the Guangdong Basic and Applied Basic Research Foundation (2020A1515110411), Maoming City Science and Technology Plan Project (200409134558218), the Open Fund of Guangdong Provincial Key Laboratory of Petrochemical Pollution Process and Control (2018B030322017) and the Projects of Talents Recruitment of GDUPT (518161).

## Notes and references

- 1 M. Kamali, M. Khalifeh, A. Saasen, R. Godøy and L. Delabroy, *J. Pet. Sci. Eng.*, 2021, **201**, 108455.



- 2 M. Bagheri, S. M. Shariatipour and E. Ganjian, *Constr. Build. Mater.*, 2018, **186**, 946–968.
- 3 X. Pang, J. Qin, L. Sun, G. Zhang and H. Wang, *Cem. Concr. Res.*, 2021, **144**, 106424.
- 4 M. R. Dousti, Y. Boluk and V. Bindiganavile, *Constr. Build. Mater.*, 2019, **205**, 456–462.
- 5 S. Adjei and S. Elkatatny, *J. Pet. Sci. Eng.*, 2021, **198**, 108201.
- 6 J. Plank, C. Tiemeyer, D. Bülischen and N. Recalde Lummer, *SPE Drill. Completion*, 2013, **28**, 398–404.
- 7 R. B. Ledesma, N. F. Lopes, K. G. Bacca, M. K. de Moraes, G. dos Santos Batista, M. R. Pires and E. M. da Costa, *J. Pet. Sci. Eng.*, 2020, **185**, 106656.
- 8 Z. Zhang, B. Zhang and P. Yan, *Constr. Build. Mater.*, 2016, **105**, 82–93.
- 9 J. Yajun and J. H. Cahyadi, *Cem. Concr. Res.*, 2003, **33**, 1543–1548.
- 10 R. Siddique, *Resour., Conserv. Recycl.*, 2011, **55**, 923–932.
- 11 N. B. Singh, M. Kalra, M. Kumar and S. Rai, *J. Therm. Anal. Calorim.*, 2015, **119**, 381–389.
- 12 Y. Wang, Z. Xu, J. Wang, Z. Zhou, P. Du and X. Cheng, *J. Therm. Anal. Calorim.*, 2020, **140**, 2225–2235.
- 13 G. Land and D. Stephan, *J. Mater. Sci.*, 2012, **47**, 1011–1017.
- 14 N. Farzadnia, H. Noorvand, A. M. Yasin and F. N. A. Aziz, *Constr. Build. Mater.*, 2015, **95**, 636–646.
- 15 L. P. Singh, S. K. Bhattacharyya, S. P. Shah, G. Mishra, S. Ahalawat and U. Sharma, *Constr. Build. Mater.*, 2015, **74**, 278–286.
- 16 A. Katende, N. V. Boyou, I. Ismail, D. Z. Chung, F. Sagala, N. Hussein and M. S. Ismail, *Colloids Surf., A*, 2019, **577**, 645–673.
- 17 S. Hatami, T. J. Hughes, H. Sun, H. Roshan and S. D. Walsh, *J. Pet. Sci. Eng.*, 2021, **207**, 109155.
- 18 Y. Reches, K. Thomson, M. Helbing, D. S. Kosson and F. Sanchez, *Constr. Build. Mater.*, 2018, **167**, 860–873.
- 19 T. Tadano, R. Zhu, Y. Muroga, T. Hoshi, D. Sasaki, S. Yano and T. Sawaguchi, *Chem. Lett.*, 2014, **43**, 705–707.
- 20 C. Zhuang and Y. Chen, *Nanotechnol. Rev.*, 2019, **8**, 562–572.
- 21 L. E. Zapata, G. Portela, O. M. Suárez and O. Carrasquillo, *Constr. Build. Mater.*, 2013, **41**, 708–716.
- 22 B. Sarde and Y. D. Patil, *Mater. Today: Proc.*, 2019, **18**, 3780–3790.
- 23 R. J. Flatt and Y. F. Houst, *Cem. Concr. Res.*, 2001, **31**, 1169–1176.
- 24 D. Jansen, J. Neubauer, F. Goetz-Neunhoeffler, R. Haerzschel and W. D. Hergeth, *Cem. Concr. Res.*, 2012, **42**, 327–332.
- 25 S. Sha, M. Wang, C. Shi and Y. Xiao, *Constr. Build. Mater.*, 2020, **233**, 117257.
- 26 M. Kremieniewski, *Energies*, 2020, **13**, 5441.
- 27 S. Mallakpour and M. Naghdi, *Prog. Mater. Sci.*, 2018, **97**, 409–447.
- 28 R. Hsissou, R. Seghiri, Z. Benzekri, M. Hilali, M. Rafik and A. Elharfi, *Compos. Struct.*, 2021, **262**, 113640.
- 29 S. Pourhashem, F. Saba, J. Duan, A. Rashidi, F. Guan, E. G. Nezhad and B. Hou, *J. Ind. Eng. Chem.*, 2020, **88**, 29–57.
- 30 K. Senthilkumar, N. Saba, N. Rajini, M. Chandrasekar, M. Jawaid, S. Siengchin and O. Y. Alotman, *Constr. Build. Mater.*, 2018, **174**, 713–729.
- 31 V. Datsyuk, S. Trotsenko, G. Trakakis, A. Boden, K. Vyzas-Asimakopoulos, J. Parthenios and K. Papagelis, *Polym. Test.*, 2020, **82**, 106317.
- 32 X. Wang, L. Wang, Q. Su and J. Zheng, *Compos. Sci. Technol.*, 2013, **89**, 52–60.
- 33 J. Chen and X. Gao, *Diamond Relat. Mater.*, 2019, **100**, 107571.
- 34 H. Gao, J. Wang, X. Chen, G. Wang, X. Huang, A. Li and W. Dong, *Nano Energy*, 2018, **53**, 769–797.
- 35 L. Lin, H. Ning, S. Song, C. Xu and N. Hu, *Compos. Sci. Technol.*, 2020, **192**, 108102.
- 36 R. Hsissou, M. Berradi, M. El Bouchti, A. El Bachiri and A. El Harfi, *Polym. Bull.*, 2019, **76**, 4859–4878.
- 37 A. Arabpour, A. Shockravi, H. Rezaia and R. Farahati, *Surf. Interfaces*, 2020, **18**, 100453.
- 38 Y. J. Kim, S. W. Ha, S. M. Jeon, D. W. Yoo, S. H. Chun, B. H. Sohn and J. K. Lee, *Langmuir*, 2010, **26**, 7555–7560.
- 39 S. Mallakpour and M. Naghdi, *Polym. Bull.*, 2016, **73**, 1701–1717.
- 40 Q. Huang, M. Liu, L. Mao, D. Xu, G. Zeng, H. Huang and Y. Wei, *J. Colloid Interface Sci.*, 2017, **499**, 170–179.
- 41 Y. Zhao, Z. Chen, X. Zhu and M. Möller, *Macromolecules*, 2016, **49**, 1552–1562.
- 42 M. Liu, J. Lei, L. Guo, X. Du and J. Li, *Thermochim. Acta*, 2015, **613**, 54–60.
- 43 Y. Qing, Z. Zenan, K. Deyu and C. Rongshen, *Constr. Build. Mater.*, 2007, **21**, 539–545.
- 44 Z. Wu, K. H. Khayat and C. Shi, *Cem. Concr. Res.*, 2017, **95**, 247–256.
- 45 G. Collodetti, P. J. Gleize and P. J. Monteiro, *Constr. Build. Mater.*, 2014, **54**, 99–105.
- 46 A. Katende, Y. Lu, A. Bunger and M. Radonjic, *J. Nat. Gas Sci. Eng.*, 2020, **79**, 103328.
- 47 M. M. Mokhtar, S. A. Abo-El-Enein, M. Y. Hassaan, M. S. Morsy and M. H. Khalil, *Constr. Build. Mater.*, 2017, **138**, 333–339.
- 48 B. Pang, Z. Zhou and H. Xu, *Constr. Build. Mater.*, 2015, **84**, 454–467.
- 49 F. K. Saleh and C. Teodoriu, *J. Energy Resour. Technol.*, 2022, **144**, 033003.
- 50 M. Nehdi and M. A. Rahman, *Cem. Concr. Res.*, 2004, **34**, 1993.
- 51 M. R. Rostami, F. Abbassi-Sourki and H. Bouhendi, *Constr. Build. Mater.*, 2019, **201**, 159–170.

